

Responses of Slender RC Columns under Cyclic Loads Considering the Effect of High Axial Compression Load [†]

Phu-Anh-Huy Pham ^{1,2,*} and Chung-Chan Hung ³¹ Institute of Research and Development, Duy Tan University, Da Nang 550000, Vietnam² Faculty of Civil Engineering, Duy Tan University, Da Nang 550000, Vietnam³ Department of Civil Engineering, National Cheng Kung University, 1 University Rd., Tainan City 701, Taiwan; cchung@ncku.edu.tw

* Correspondence: phampanh Huy@duytan.edu.vn

[†] Presented at the 1st International Online Conference on Buildings, 24–26 October 2023; Available online: <https://iocbd2023.sciforum.net/>.

Abstract: Modern tall and irregular buildings have become increasingly slender and have columns with high axial force, which can pose a serious risk to the seismic safety of these structures. However, existing experimental studies on slender reinforced concrete (RC) columns under high axial force are limited due to the restrictions of testing facilities. Most studies are based on small cross-section specimens bent in single curvatures and loaded monotonically. But these studies may not accurately reflect the realistic seismic behavior of full-scale double-curvature RC columns in buildings due to size effects. Therefore, the objective of this study is to provide new insights into the seismic performance of full-scale slender and large cross-section RC columns with various transverse reinforcement designs under a constant high axial load of up to 50% of the axial capacity. The full-scale specimens were tested in a double-curvature configuration under cyclic lateral displacement reversals and high axial loads. The results show that the tested slender columns experienced significant P- Δ moment magnification effects with further drifts after yielding. This imposed a greater loading demand on the sections and destabilized the columns after peak loads. The robustly anchored transverse reinforcement improved seismic performance indicators, including strength retention and drift capacity, and reduced the P- Δ moment magnification experienced by slender columns, which enhances the stability index.

Keywords: Slender RC column; high compression axial load; transverse reinforcement; P- Δ effect; moment magnification; stability index

Citation: Pham, P.-A.-H.; Hung, C.-C. Responses of Slender RC Columns under Cyclic Loads Considering the Effect of High Axial Compression Load. *Eng. Proc.* **2023**, *53*, x. <https://doi.org/10.3390/xxxxx>

Academic Editor(s): Name

Published: 24 October 2023



Copyright: © 2023 by the authors. Submitted for possible open access publication under the terms and conditions of the Creative Commons Attribution (CC BY) license (<https://creativecommons.org/licenses/by/4.0/>).

1. Introduction

The development of high-strength concrete and steel reinforcing bars facilitates the use of slender load-bearing members [1]. However, the dual demands of a small cross-section and high axial load have raised critical concerns about the limit state designs for slender reinforced concrete (RC) columns in high-seismic regions [2–4]. The resistance of slender RC columns to lateral loads is controlled by the cross-sectional capacity and slenderness of the column. A large slenderness ratio causes a significant reduction in the lateral load resistance of RC columns due to the magnified $P - \Delta$ effect upon the lateral deformation. Particularly, the second-order moment of slender RC columns is amplified with the increasing axial compression. In addition to the slenderness ratio and axial load demand, the second-order moment calculated per ACI 318-19 is also magnified with the reduced structural stiffness due to concrete cracking, which could become significant at a high ductility demand [5]. Hence, an appropriate seismic design of slender RC columns requires knowledge of the interacting effects of the axial compression, slenderness ratio, and ductility demand.

Some researchers studied on slender RC columns such as Kim et al. [6] conducted a series of axial tests on 30 scaled RC columns (having a cross-section of 80 × 80 mm) with the slenderness ratios (λ) of 10, 60, and 100. Wibowo et al. [7] experimentally investigated the behavior of four scaled single-curvature slender columns (having a cross-section of 270 × 300 mm with $\lambda = 28$) under cyclic lateral loading. Similarly, Esmaelly and Xiao [8] also demonstrated that a higher axial load demand reduced the ductility of the circular columns with a diameter of 406 mm and $\lambda = 36$. Senner et al. [9] experimentally investigated the size effect on the behavior of slender RC columns subject to cyclic lateral loads using 27 RC columns with a square cross-section of 50–200 mm and a slenderness ratio of 10–35. Existing studies on slender RC columns often adopted scaled specimens subject to single-curvature bending and monotonic loading). Notably, while the slender RC columns with light reinforcement and high axial load demand can be widely found in old buildings, their seismic and failure behavior is yet to be sufficiently understood. To fill the knowledge gap, this study experimentally explored the response of large-scale, slender RC columns under lateral displacement reversals and high axial loads. The column specimens were tested in double-curvature bending to reflect better the actual boundary conditions of RC columns in a frame. The study’s objective was to investigate the effects of high ALRs and transverse reinforcement detailing on the seismic behavior of slender RC columns at different limit states. The behavior of the slender columns under the influence of $P - \Delta$ effects was extensively discussed in terms of the failure pattern, hysteretic response, strength and stiffness degradation, displacement component, and structural stability. In addition to the experimental study, the applicability of existing evaluation methods for the effective stiffness, moment magnification factor, and stability index of the tested slender RC columns was assessed.

2. Experimental Program

2.1. Specimen Design

Three large-scale RC columns (namely NC1-0.5P, NC2-0.5P, and NC3-0.1P) with a cross-section of 400 × 400 mm, clear height of 3000 mm, and slenderness ratio of 26.0 were fabricated and tested. Columns NC1-0.5P and NC2-0.5P were subjected to a high ALR of 0.5, while NC3-0.1P was assigned a low ALR of 0.1. The low and high ALR values were deliberately chosen to position them at the upper and lower balance point of P-M interaction diagram, respectively. The design details are shown in Figure 1 and summarized in Table 1. The compressive strength of the concrete materials was determined on the test days of the columns using three 150 × 300 mm cylinders which were cast using the same batch for the columns. The compressive tests on the cylinders were conducted using the standard test procedure conforming to ASTM-C39 [10]. The longitudinal and transverse reinforcement of the columns had a nominal yield strength of 420 MPa. Their actual yield strengths were determined using uniaxial tensile tests on steel coupons.

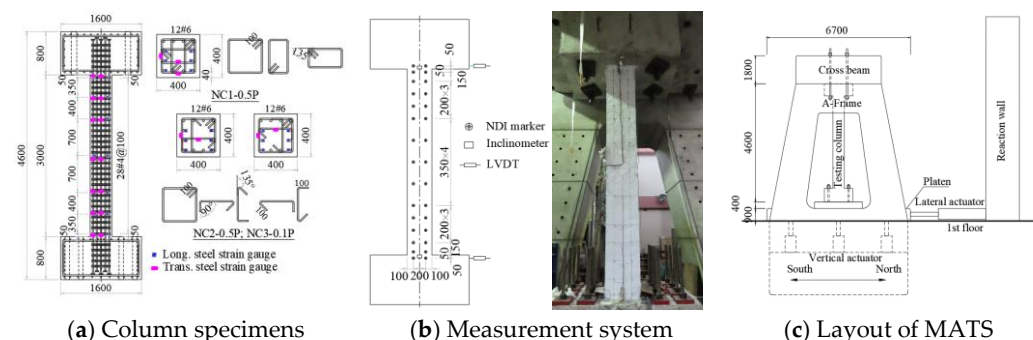


Figure 1. Specimen design and measurement system.

The detailed design parameters are presented in Table 1. The two ends of each column were connected to RC blocks. The RC blocks had a dense array of reinforcement and depth to restrain their potential damage and deformation during structural tests and allow the longitudinal reinforcement of the columns to have sufficient development length. In Table 1, the nominal shear strength of the columns was calculated according to ACI 318-19 [11]. The nominal flexural strength of the columns was determined using the moment-curvature analysis with the fiber section model in OpenSEES [12]. The steel bars were modeled using a bilinear strain-hardening material. Details of the fiber section model can be found in [13]. The material parameters were determined according to the results of material tests. All columns were designed to fail in a flexure-controlled mode. The ratio of the shear demand at the nominal flexural strength (V_{mn}) to the nominal shear strength (V_n) was less than 0.4 for the columns [14–17].

Table 1. Column design parameters.

Specimens	Concrete f'_c (MPa)	Axial Load Ratio	Longitudinal Reinforcement			Transverse Reinforcement			$\frac{V_{mn}}{V_n}$
			f_y (MPa)	Bars	Bar Size	s (mm)	f_{yv} (MPa)	$\frac{\rho_v f_{yv}}{f'_c}$	
NC1-0.5P	49.7	0.5	475	12#6	#4	100	470	0.121	0.27
NC2-0.5P	49.7								0.32
NC3-0.1P	51.9	0.1						0.087	0.27

2.2. Test Setup and Instrumentation

The columns were tested by a multi-axial test system (MATS), as shown in Figure 2. The MATS is a 6-DOF loading system for seismic testing of large-scale structural components. It has two sets of vertical and horizontal actuators with capacities of 30MN and 4.5MN, respectively [18]. The columns were installed in the test system with their top and bottom RC blocks fixed onto the steel plates of the MATS through multiple pre-stressed high-strength steel rods, as shown in Figure 2.

Different measurement devices were adopted to monitor the detailed response of the columns. The displacement field of the column specimens was monitored using an Optotrak Certus optical measurement system. The locations of the NDI markers (light sensors) are shown in Figure 1b. The markers were more concentrated at the top and bottom of the columns, where plastic hinges were expected to develop. A dense array of strain gauges was also used during the tests to record the strain development in the longitudinal and transverse reinforcement. The deployment of the strain gauges is shown in Figure 1a. Furthermore, the possible displacement and rotation of the top and bottom RC blocks were monitored using linear variable displacement transformers (LVDTs) and inclinometers.

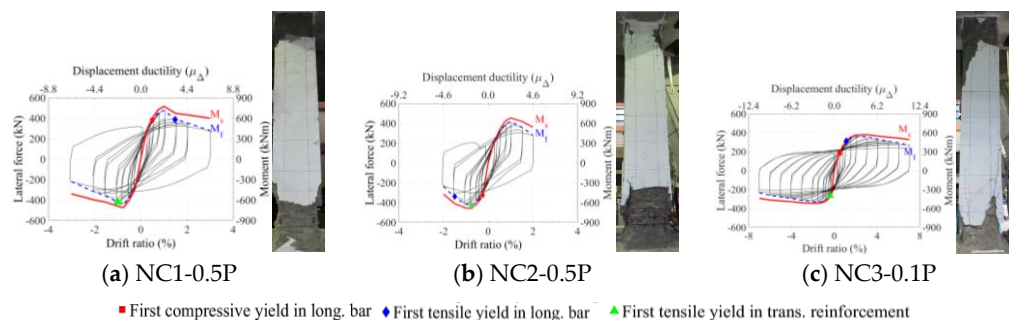


Figure 2. Hysteresis loops and damage patterns of the columns.

3. Experimental Results

3.1. Damage Pattern

Figure 2 shows the damage patterns of the columns at the peak load and failure. It was observed during the tests that a higher axial load demand suppressed the formation of cracks. Although NC3-0.1P had no vertical splitting cracks due to its low axial load demand, it had substantially more flexural cracks compared to the high ALR columns. At the peak load, the three high ALR columns exhibited similar cracking patterns despite the difference in the amount and detailing of the transverse reinforcement, due to the small shear demand of the slender columns. However, NC1-0.5P had less concrete spalling than NC2-0.5P at the peak load. This result implies that the enhanced confinement effect provided by the higher transverse reinforcement ratio as per ACI318-19 was beneficial for slender RC columns to restrain concrete crushing. Substantial concrete crushing and spalling occurred to all columns at the ultimate limit state, especially for the high ALR columns, as shown in Figure 2. The significant concrete spalling and high axial demand in NC2-0.5P caused the opening of the 90-degree hooks, which were designed as per ACI318-11, and buckling of the longitudinal rebar. Hence, the use of a more robust transverse reinforcement detailing (i.e., a combination of three closed hoops with 135-degree hooks) in NC1-0.5P evidently led to improved confinement on the concrete core and greater lateral support to the longitudinal bars compared to the use of crossties with 90-degree hooks at an equivalent reinforcing ratio. For NC3-0.1P with a low ALR, the longitudinal rebar buckled after gradual concrete crushing, although its 90-degree hooks were not open during the test. At the end of the tests, the 135-degree hooks in all columns remained closed. No fracture was observed for the transverse reinforcement in all columns, which could be attributed to the low shear demand of the slender columns.

3.2. Load-Displacement Behavior

The load-displacement hysteretic responses (in solid black lines) of the columns are presented in Figure 2. For investigating the axial load-slenderness interacting effect on the columns' behavior, the evolutions of the first-order moment M_f (in dashed-blue lines, calculated directly based on the applied lateral force) and the magnified moments M_s (in solid-red lines, equal to M_f plus the $P - \Delta$ moment) over the displacement demands are also plotted in Figure 2.

All columns reached their nominal flexural strengths prior to failure. The two high ALR columns had similar drifts at the peak loads between 0.75% and 1.0%. In contrast, NC3-0.1P's drift at the peak load was about two times higher, reaching 2% despite the lower peak strength. As shown in Figure 2, the high axial compression significantly delayed the tensile yielding of the longitudinal rebar, which firstly yielded in compression for columns with ALR = 0.5. Meanwhile, the longitudinal rebar of NC3-0.1P almost concurrently yielded in both tension and compression, which increased the column's deformability and ductility.

The peak strength of NC1-0.5P was 11.4% greater than that of NC2-0.5P. Hence, the enhanced confinement effect by replacing the crossties with the closed hoops was beneficial in sustaining the stability of the slender columns and improving the core concrete strength after cracking and spalling occurred, thus promoting flexural strength development. In contrast to NC1-0.5P with the higher peak strength and ductility, columns NC2-0.5P displayed similar brittle load-displacement behavior with the lower peak strength. The poorer seismic performances of NC2-0.5P suggested that the non-robust crossties could not provide effective confinement to the concrete core and restrain the buckling of the longitudinal rebar of slender RC columns.

The high ALR of 0.5 caused the post-peak strength of the slender columns to degrade rapidly with the increased drift demand due to the destabilizing effect of the $P - \Delta$ moment and the increased compressive stress that led to early concrete crushing and rebar buckling. As a result, all three high ALR columns did not have an obvious post-peak

plateau in the load-drift hysteretic loops despite their low V_{mn}/V_n values. The drift capacity was defined as the drift ratio when the retained strength was 85% of the peak strength ($0.85V_{max}$) [14,16,19]. The ALR effect on the drift capacity of the column was well observed by comparing the results of NC2-0.5P and NC3-0.1P. The drift capacity decreased significantly from 6.9% to 1.7% when the ALR increased from 0.1 to 0.5 as a result of the more substantial concrete crushing and $P - \Delta$ effect.

4. Stability and Ductility

4.1. Moment Magnifiers

The $P-\Delta$ effect under high axial compression can increase the moment demand on the section and also lead to instability of unbraced slender columns. The contribution of $P-\Delta$ magnified moments to the total moment experienced by the columns at different drift levels is shown in Figure 10. The results show that the $P-\Delta$ moment became non-negligible after the yielding occurred and was significant after the peak strength. To further quantify the influence of the $P-\Delta$ magnified moment, the moment magnifiers, i.e., M_s/M_f , of the four columns at different drift levels are plotted and compared in Figure 4b. It can be seen that a larger ALR and drift demand led to a higher moment magnification. Despite the high slenderness of the column, the moment magnification of NC3-0.1P was minor due to the small axial load demand. It was 1.03 and 1.1 at the 1% and 4% drift ratios, respectively.

Figure 3b shows that in contrast to the minor moment magnification (less than 1.1) prior to 1% drift at which the peak strength was nearly reached, the $P-\Delta$ action became more profound for the post-peak behaviors. Comparing the three high ALR columns, column NC1-0.5P had a slightly lower moment magnification. For example, at 2% drift, NC1-0.5P and NC2-0.5P had a moment magnification factor of 1.2 and 1.4, respectively. The lesser moment magnification could be due to its enhanced core confinement with the closed hoops that improved the stiffness retention in NC1-0.5P. This result is consistent with the moment magnifier model in ACI 318-19, in which a higher effective stiffness leads to smaller moment magnification. In summary, to satisfy the general equilibrium of the slender columns with high ALR, the results suggest the necessity to consider the $P-\Delta$ effect. Otherwise, loss of moment capacity for resisting lateral loads can be caused by the moment magnifications due to the $P-\Delta$ effects.

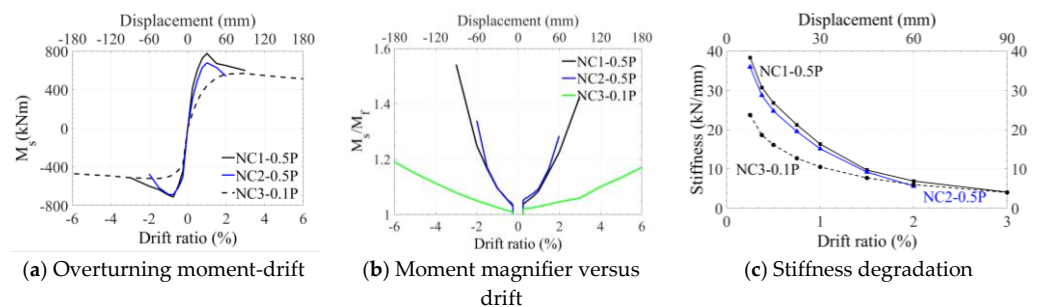


Figure 3. Influence of drift demand on the overturning moment and moment magnification factor δ_s , and stiffness degradation.

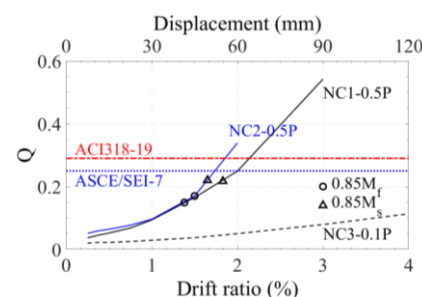


Figure 4. The influence of drift demand on the stability index.

4.2. Stiffness Degradation

Lateral stiffness is directly related to the moment magnification and stability issues of the columns under significant P- Δ effects. The axial compression would incur a negative geometric stiffness [20], reducing the apparent lateral stiffness and destabilizing the columns. Under cyclic loading, the stiffness of columns would degrade continuously with the accumulated damage, and that poses a further risk to the column stability. The secant stiffness of the tested columns at different drift levels was calculated and presented in Figure 3c. The secant stiffness at a specified target drift was computed as the slope between the load-displacement points at the positive and negative extremes during the 1st loading cycle. Figure 3c shows that NC-0.1P had an initial stiffness that was approximately 34% lower than that for the high ALR columns due to its lower axial load demand. However, the high axial compression caused a more rapid drop in the stiffness as the drift increased because of the more significant concrete crushing and the P-delta effect. At 1.5% drift, all columns had comparable secant stiffness.

As for the influence of the steel confinement, the initial stiffness of NC1-0.5P was about 10% higher than that of NC2-0.5P. The higher stiffness of NC1-0.5P implies that using closed hoops to replace cross-ties could enhance the confinement on the core concrete after initial cracking. Prior to 1% drift (at which the peak strength occurred), NC1-0.5P consistently had the greatest stiffness among the tested columns.

4.3. Displacement Ductility

The displacement ductility factor (μ) of the tested column specimens was calculated as the ratio of the ultimate displacement (Δ_u) and yield displacement (Δ_y). The yield and ultimate displacements were estimated according to [21,22]. The yield displacement was calculated as the displacement corresponding to the intersection of the maximum lateral load and secant stiffness at 75% of the maximum lateral load. The ultimate displacement was obtained when the lateral strength dropped by 15% from the maximum lateral strength. The calculated displacement ductility factors of the slender RC columns are summarized in Table 2.

For the two high ALR columns, NC1-0.5P had the higher displacement ductility of 3.9. Greater confinement of the transverse reinforcement increased the yield and ultimate displacements, whereas it only negligibly enhanced the ductility factor of slender RC columns. In contrast to the relatively minor influence of the transverse reinforcement design for the slender columns, the ALR significantly impacted the yield and ultimate displacements as well as the displacement ductility factor. Reducing the ALR from 0.5 in NC2-0.5P to 0.1 in NC3-0.1P increased the yield and ultimate displacements by 1.5 and 4.1 times, respectively. It also improved the displacement ductility factor from 3.8 to 10.6 due to the reduced second-order moment and concrete crushing.

Table 2. The displacement ductility factors.

Columns	Test Results		
	Δ_y^* (mm)	Δ_u^* (mm)	μ
NC1-0.5P	13.6	52.5	3.9
NC2-0.5P	13.1	49.8	3.8
NC3-0.1P	19.4	206.0	10.6

* The averages of the Δ_y and Δ_u in the positive and negative cycles are presented.

4.4. Stability Index

In addition to conventional damage limit states mostly related to material properties, slender columns have a limit that marks the onset of structural instability. The stability limit may define the ultimate response condition for a slender column before significant

material-related damage is observed. Different stability limits, e.g., ASCE/SEI-7 [23], ACI318-19 [11], have been proposed. In ACI318, the stability index Q is given as:

$$Q = \frac{P\Delta}{Vl_c} \quad (1)$$

where Δ is the lateral displacement; V is the lateral force; and l_c is the length of column. According to ASCE/SEI-7 [23], the maximum value of the stability coefficient is about 0.25, which is equivalent to a P - Δ magnified-to-primary moment ratio of 1.33. ACI 318 defines the upper limit of 1.4 on the magnified-to-primary moment ratio, which is equivalent to $Q = 0.29$.

Figure 4 presents the stability index Q following ACI318-19's equation of all columns and two criteria, i.e., ASCE-SEI-7 [23] and ACI318-19 [11]. It can be seen that the stability index of the high ALR columns reached 0.2 prior to the ultimate limit state (i.e., $0.85V_{peak}$). Analytical study [24] on reinforced concrete frames showed that the probability of stability failure increases rapidly when the stability index Q exceeds 0.2. NC2-0.5P and NC1-0.5P had comparable stability indexes prior to 1.5% drift. These columns reached ACI 318's stability limit at 1.9% and 2.2% drift, respectively, implying that the enhanced concrete confinement enhances structural stability at the ultimate limit state. On the other hand, due to the small influence of $P - \Delta$ effects under the low compression load, NC3-0.1P columns did not reach any limit index until the end of testing.

5. Conclusions

This paper presents a comprehensive experimental investigation of the cyclic responses of full-scale slender RC columns under high axial compression load. All columns reached their nominal flexural strengths with longitudinal and transverse reinforcements yielded prior to failure. The slender columns' failure mode and hysteretic responses were significantly affected by the ALR and transverse reinforcement design. Based on the test results, the following conclusions are drawn:

- (1) Increasing the ALR from 0.1 to 0.5 substantially reduced the peak drift ratio of as much as 3% (NC3-0.1P) to 0.75% (NC2-0.5P). Substantial concrete crushing and spalling occurred to all columns at the ultimate limit state, especially for the high ALR columns.
- (2) Increasing the ALR from 0.1 to 0.5 increased the peak strength by 21% and initial stiffness by 86% but caused the stiffness and post-peak strength to degrade rapidly due to the significant concrete compression demand and $P - \Delta$ effect. It also significantly reduced the drift capacity by 76% and displacement ductility by 64%.
- (3) Effective core confinement by robust transverse reinforcement with 135-degree hooks and closed hoops was essential to sustain the stability of the slender columns and improve flexural strength development, strength and stiffness retention, drift capacity, and displacement ductility. It also effectively enhanced the lateral support to the longitudinal bars, preventing rebar buckling after concrete crushing.
- (4) The P - Δ effects became noticeable after the yielding and significantly affected the post-peak response. The enhanced steel confinement by replacing 90-degree cross-ties with 135-degree closed hoops reduced the moment magnification factor from 1.45 to 1.20 at the ultimate limit state.
- (5) The stability index of the high ALR columns reached 0.2 prior to the ultimate limit state, which was indicative of the rapidly increased probability of stability failure. The high ALR columns reached ACI 318's stability limit at 1.75–2.2% drift. Robust transverse reinforcement detailing was beneficial in enhancing the structural stability for slender RC columns under high compression demand at the ultimate limit state.

Nevertheless, the scope of the paper was limited to the analysis of conventional slender columns (with normal slenderness) featuring rectangular cross-sections. It is crucial

that forthcoming research undertakes a comprehensive exploration of slender columns characterized by high slenderness ratios and diverse cross-sectional geometries.

Author Contributions: Conceptualization, P.-A.-H.P. and C.-C.H.; methodology, P.-A.-H.P. and C.-C.H.; software, P.-A.-H.P.; validation, P.-A.-H.P. and C.-C.H.; formal analysis, P.-A.-H.P. and C.-C.H.; investigation, P.-A.-H.P. and C.-C.H.; resources, P.-A.-H.P. and C.-C.H.; data curation, P.-A.-H.P. and C.-C.H.; writing—original draft preparation, P.-A.-H.P.; writing—review and editing, C.-C.H.; visualization, P.-A.-H.P. and C.-C.H.; supervision, C.-C.H.; project administration, C.-C.H.; funding acquisition, C.-C.H. All authors have read and agreed to the published version of the manuscript.

Funding: This study was sponsored in part by the Ministry of Science and Technology, Taiwan, under Grant No. 109-2636-E-006-015.

Informed Consent Statement: Written informed consent has been obtained from the patient(s) to publish this paper.

Acknowledgments: The support from the Ministry of Science and Technology and the National Center for Research on Earthquake Engineering NCREE is greatly appreciated by the authors.

Conflicts of Interest: The authors declare no conflict of interest.

References

1. Mendis, P. Design of high-strength concrete members: State-of-the-art. *Prog. Struct. Eng. Mater.* **2003**, *5*, 1–15. <https://doi.org/10.1002/pse.138>.
2. Yuen, Y.P.; Kuang, J.S. Effect of axial compression on ductility design of RC walls. *Proc. Inst. Civ. Eng. -Struct. Build.* **2015**, *168*, 554–569. <https://doi.org/10.1680/stbu.14.00024>.
3. Yuen, T.Y.P.; Kuang, J.S. Revisiting the effect of axial force ratio on the seismic behaviour of RC building columns. *Struct. Eng. Int.* **2017**, *27*, 88–100. <https://doi.org/10.2749/101686617X14676303589273>.
4. Park, S.; Mosalam, K.M. Experimental Investigation of Nonductile RC Corner Beam-Column Joints with Floor Slabs. *J. Struct. Eng.* **2013**, *139*, 1–14. [https://doi.org/10.1061/\(ASCE\)ST.1943-541X.0000591](https://doi.org/10.1061/(ASCE)ST.1943-541X.0000591).
5. Kwon, J.; Ghannoum, W.M. Assessment of international standard provisions on stiffness of reinforced concrete moment frame and shear wall buildings. *Eng. Struct.* **2016**, *128*, 149–160. <https://doi.org/10.1016/j.engstruct.2016.09.025>.
6. Kim, J.-K.; Yang, J.-K. Buckling behaviour of slender high-strength concrete columns. *Eng. Struct.* **1995**, *17*, 39–51. [https://doi.org/10.1016/0141-0296\(95\)91039-4](https://doi.org/10.1016/0141-0296(95)91039-4).
7. Wibowo, A.; Wilson, J.L.; Lam, N.T.K.; Gad, E.F. Drift capacity of lightly reinforced concrete columns. *Aust. J. Struct. Eng.* **2014**, *15*, 131–150.
8. Esmaeily, A.; Xiao, Y. Behavior of reinforced concrete columns under variable axial loads: Analysis. *ACI Struct. J.* **2005**, *102*, 736–744. <https://doi.org/10.14359/14669>.
9. Şener, S.; Barr, B.I.G.; Abusiaf, H.F. Size Effect in Axially Loaded Reinforced Concrete Columns. *J. Struct. Eng.* **2004**, *130*, 662–670. [https://doi.org/10.1061/\(ASCE\)0733-9445\(2004\)130:4\(662\)](https://doi.org/10.1061/(ASCE)0733-9445(2004)130:4(662)).
10. ASTM C39; Standard Test Method for Compressive Strength of Cylindrical Concrete Specimens. Annual Book of ASTM Standards. 2005.
11. ACI Committee 318. *Building Code Requirements for Structural Concrete*; ACI: Farmington Hills, MI, USA, 2019.
12. Mazzoni, S.; McKenna, F.; Scott, M.H.; Fenves, G.L. *OpenSees Command Language Manual*; University of California: Berkeley, CA, USA, 2006.
13. Hung, C.-C.; Lu, W.-T. A Performance-Based Design Method for Coupled Wall Structures. *J. Earthq. Eng.* **2017**, *21*, 579–603. <https://doi.org/10.1080/13632469.2016.1172379>.
14. Anh Huy, P.P.; Yuen, T.Y.P.; Hung, C.-C.; Mosalam, K.M. Seismic behaviour of full-scale lightly reinforced concrete columns under high axial loads. *J. Build. Eng.* **2022**, *56*, 104817. <https://doi.org/10.1016/j.job.2022.104817>.
15. Yuen, T.Y.P.; Wen, T.-H.; Hung, C.-C.; Zhang, H.; Pham, P.A.H.; Deng, Y. An eigendecomposition-based and mesh-sensitivity reduced constitutive model for nonlinear analysis of concrete structures under non-proportional cyclic loading. *J. Build. Eng.* **2022**, *47*, 103875. <https://doi.org/10.1016/j.job.2021.103875>.
16. Pham, H.P. Shear strength model of large-scale reinforced concrete rectangular columns with light transverse reinforcement. *Asian J. Civ. Eng.* **2022**, *24*, 219–244. <https://doi.org/10.1007/s42107-022-00499-9>.
17. Pham, P.-A.-H.; Hung, C.-C. Assessment of plastic hinge length in reinforced concrete columns. *Struct. Infrastruct. Eng.* **2023**, 1–16. <https://doi.org/10.1080/15732479.2023.2263432>.
18. Chen, J.C.; Lin, T.H.; Chen, P.C.; Lin, K.C.; Tsai, K.C. Advanced seismic testing using the multi-axial testing system (MATS) in NCREE. In Proceedings of the International Conference on Advances in Experimental Structural Engineering, October, Eucentre; 2009; Volume 2009.

19. Sezen, H.; Moehle, J.P. Shear strength model for lightly reinforced concrete columns. *J. Struct. Eng.* **2004**, *130*, 1692–1703. [https://doi.org/10.1061/\(ASCE\)0733-9445\(2004\)130:11\(1692\)](https://doi.org/10.1061/(ASCE)0733-9445(2004)130:11(1692)).
20. Wilson, E.L.; Habibullah, A. Static and Dynamic Analysis of Multi-Story Buildings, Including P-Delta Effects. *Earthq. Spectra* **1987**, *3*, 289–298. <https://doi.org/10.1193/1.1585429>.
21. Priestley, M.J.N.; Park, R. Strength of Ductility of Concrete Bridge Columns Under Seismic Loading. *ACI Struct. J.* **1987**, *84*, 61–76. <https://doi.org/10.14359/2800>.
22. Park, R. Evaluation of ductility of structures and structural assemblages from laboratory testing. *Bull. N. Z. Soc. Earthq. Eng.* **1989**, *22*, 155–166. <https://doi.org/10.5459/bnzsee.22.3.155-166>.
23. ASCE. *Seismic Evaluation and Retrofit of Existing Buildings (41-17)*; American Society of Civil Engineers: Reston, VA, USA, 2017.
24. MacGregor, J.G.; Hage, S.E. Stability Analysis and Design of Concrete Frames. *J. Struct. Div.* **1977**, *103*, 1953–1970. <https://doi.org/10.14359/51685164>.

Disclaimer/Publisher’s Note: The statements, opinions and data contained in all publications are solely those of the individual author(s) and contributor(s) and not of MDPI and/or the editor(s). MDPI and/or the editor(s) disclaim responsibility for any injury to people or property resulting from any ideas, methods, instructions or products referred to in the content.